Construction and Building Materials 271 (2021) 121548

Contents lists available at ScienceDirect

Construction and Building Materials

journal homepage: www.elsevier.com/locate/conbuildmat

In-plane behaviour of rubble stone masonry walls: Experimental, numerical and analytical approach

João M. Pereira [a,*], António A. Correia [b], Paulo B. Lourenço [a]

[a] ISISE, Department of Civil Engineering, University of Minho, Guimarães, Portugal
[b] LNEC, National Laboratory for Civil Engineering, Lisbon, Portugal

HIGHLIGHTS

- In-plane non-linear numerical models for rubble stone masonry walls.
- A parametric study is presented for in-plane rubble stone masonry walls.
- Comparison of analytical models for predicting shear strength of masonry walls.

ARTICLE INFO

Article history:
Received 4 February 2020
Received in revised form 27 October 2020
Accepted 29 October 2020
Available online 14 November 2020

Keywords:
Rubble masonry
Shear capacity
Numerical analysis
Analytical models

ABSTRACT

Unreinforced masonry construction is predominant in many urban areas world-wide.

Many of these constructions are vulnerable to earthquakes, which are the main cause of damage and loss of cultural heritage. Understanding the in-plane behaviour of masonry walls when subjected to horizontal loadings will improve the society capacity to preserve and protect this cultural heritage. An experimental campaign on rubble stone masonry walls under different loading conditions is presented. This experimental campaign allows calibrating non-linear numerical models used to study these elements in a more comprehensive way, performing parametric studies regarding the geometry, pre-compression level, boundary conditions and mechanical properties. The capacity to estimate the shear strength using available analytical models is also reviewed, applied and compared.

1. Introduction

The increasing awareness for the preservation of the built heritage is a result of the social responsibility to protect its cultural identity, perpetuating it for future generations. Many of these constructions are vulnerable to earthquakes and its damage and collapse during a seismic event is a permanent threat to human lives.

Considering past seismic events, it has been recognized that masonry buildings are vulnerable to these actions [1–3]. Masonry buildings are usually able to sustain the vertical loads [4], however, from the structural point of view; these buildings tend to fail to respond well to seismic loads [5–7]. The seismic behaviour of a masonry building is defined by the interaction of the in-plane wall, the out-of-plane walls and the floor diaphragms through their connections. The characteristic damage patterns include: cracks at the corners and wall intersections, which occurs as a result of insufficient connections; out-of-plane bending due to lack of connections between the walls and the floors; diagonal cracking in the in-plane walls, among others. In general terms the damage in masonry buildings can be essentially interpreted by two fundamental collapse mechanisms: out-of-plane and in-plane. This work studies the in-plane collapse mechanisms of masonry walls.

According to post-earthquake surveys and experimental studies, four types of failure mechanisms define the behaviour of structural masonry walls under in-plane seismic actions: rocking and toe crushing (flexural); sliding and diagonal cracking (shear) [8,9]. Some authors [10–12] only identify three mechanisms, where the rocking and toe crushing are not considered separately, being called flexural mechanism. Rocking occurs when the wall begins to behave nearly as a rigid body rotating at its toe, usually when the vertical load is low and the horizontal load produces a flexural motion making the pier bend around the toe. Toe crushing is typically observed after rocking deformations, is usually associated with the compressive failure of masonry at the toe of the pier. Sliding is characterized by the wall deformation along a horizontal bed-joint plane, usually located at one of the extremities of the pier. Diagonal cracking usually develops in the centre of the wall and propagate toward the corners. This failure mode generally occurs in the interface between unit and mortar

* Corresponding author at: Department of Civil Engineering, University of Minho, Campus de Azurém, Guimarães 4800-058, Portugal.
E-mail address: jpereira@civil.uminho.pt (J.M. Pereira).

https://doi.org/10.1016/j.conbuildmat.2020.121548
0950-0618/

because this is often the weakest link in masonry assemblages [13]. The cracks propagate through the mortar joints or directly through the units depending on the relative strength of the bond and units. Walls will fail according to failure mode that requires the least amount of force to mobilize, and its occurrence depends mainly on the geometry, boundary conditions, pre-compression stress state and masonry mechanical properties.

Several authors studied the behaviour of masonry buildings when subjected to in-plane loading through experimental campaigns [14–24]. However, the high number of possible combinations of materials, geometry, boundary conditions, vertical loading, among others, makes the characterization of these elements a challenge. Numerical analysis can be considered auxiliary to experimental tests, allowing the assessment of masonry walls in-plane behaviour when varying some parameters without the need of extensive experimental work.

This work studies the in-plane behaviour of rubble stone masonry walls through an experimental campaign on specimens under different loading conditions, allowing calibration of non-linear numerical models. The calibrated models allow comprehensive parametric studies regarding the geometry, pre-compression level, boundary conditions and mechanical properties of the rubble stone masonry walls. This work also reviews, applies and compares different available analytical solutions to estimate the shear capacity of these elements.

2. Experimental testing

An experimental campaign was developed at the National Laboratory for Civil Engineering, Portugal (LNEC). Two rubble stone masonry walls, representative of existing buildings, were built using limestone and hydraulic lime mortar. Fig. 1 depicts the walls built for this experimental campaign, which present a central panel with dimensions 2700 × 1700 × 450 mm. Each wall is composed of over 140 stones; each stone of the wall face is not reaching even half of the thickness of the wall. Additional smaller size stones are used in between the two faces of the wall, as typical in construction type and epoch represented by the wall specimens.

Two different specimens were built using a mortar with 1:4 lime/sand ratio. This mortar was mechanically characterized and presented an average compressive strength of 0.8 MPa.

The test setup involved the use of the LNEC's shaking table (to which the base of the wall specimens was attached) and a reaction wall, as schematically represented in Fig. 1. The top of the wall was connected to the reaction wall, by means of a L-shaped steel connector which ensured that the horizontal reaction was applied at mid-height of the central test panel (Fig. 1c). The lateral movement was imposed on the wall by moving the shaking table horizontally.

Two different types of tests were performed on the specimens in terms of horizontal loading: monotonic and cyclic. In both tests the specimens were initially loaded in the vertical direction until a predetermined load was achieved using two hydraulic cylinders (jacks) having the same oil pressure between them ("C", Fig. 1). Afterwards, the specimens were loaded horizontally, by imposing the motion at the base of the specimens and with the top of the specimen fixed at point "H" (Fig. 1). In the monotonic test the specimen was horizontally loaded until failure, while in the cyclic test the specimen was subjected to a predefined series of positive and negative displacements of the shaking table. Both tests were performed under constant displacement rate of 0.2 mm/s.

2.1. Experimental results

The results for the experimental tests are presented in terms of horizontal force (measured in load cell "E", Fig. 1) and differential horizontal displacement between the top and the base of the central test panel. These displacements were measured using LVDTs (Linear Variable Differential Transformer) placed along the height of the wall.

Wall 1, was subjected to an initial vertical load of 0.15 MPa in a first phase. Later this specimen was subjected to a horizontal load until collapse. In Fig. 2a it is possible to see that this specimen failed in shear by formation of diagonal cracks. This wall presented a shear resistance of 105 kN, being this maximum force registered at a horizontal displacement of 8.95 mm (Fig. 3a).

Wall 2, was subjected to an initial vertical load of 0.20 MPa. Later, this specimen was subjected to a series of growing (positive and negative) displacements, namely 2, 5, 10, 20, 20, 20, 40 and 40 mm. Fig. 2b shows the damage pattern obtained for this specimen. It should be noted that the process in which the vertical load was applied proved to be quite challenging, and it was not possible to match both tests with the same vertical load. As it will be possible to see next, this difference (4.5% of the f_c) had little influence in the results. It is possible to see a shear failure with diagonal cracking being developed in both directions. Plotting the force–displacement curve for all the displacement series (Fig. 3b) it is possible to see that the shear resistance of this wall is 95 kN, being this maximum force registered at a positive horizontal displacement of 5.4 mm (Fig. 3c).

Observing Fig. 2 (failure mode) and Fig. 3 (force–displacement curves), and as expected, it is possible to see that the shear resistance in the monotonic test is similar to the shear resistance obtained with the cyclic test (Fig. 3d).

3. Numerical analysis

Numerical models were built to try and replicate the obtained experimental results, in order to perform parametric studies. The Finite Element Method (FEM) was chosen to perform the simulations, using DIANA 9.4 (2009) software. In order to replicate, as best as possible, the obtained experimental results, the numerical model included the masonry wall, the steel support structure on the top of the wall ("B", Fig. 1) and the steel anchors ("I", Fig. 1) being simulated using springs (Fig. 4a).

The masonry was modelled using a macromodelling approach, assuming the masonry as a composite material. This modelling strategy is an alternative to the micromodelling of the masonry components (units, mortar and interfaces) and assumes the use of average mechanical properties for masonry [25,26]. Several authors have been using this modelling strategy for masonry obtaining adequate responses for these structures and materials [27–30]. Another advantage of using this modelling strategy is the reduced computational time when compared with micro modelling, which usually required denser and complex finite element meshes [13]. This is particularly important in this presented work, as it is expected a large number of non-linear analysis for the parametric study and the analytical solutions study. In the specific case of rubble masonry, it is usually difficult to obtain detail information regarding the geometry and positioning of the units and the mortar thickness, which makes difficult the development of reliable micromodels. In our case, for each wall there are over 140 stones, meaning that both faces of the wall were not made of the same stones, rendering different results, as the micromodelling approach is heavily dependent of the geometry of the joints. Taking all of this into consideration, the macromodelling approach was used.

The FEM models used in this work were built using 2D plane stress elements. A regular mesh discretization was used using four-node quadrilateral isoparametric plane stress elements based on linear interpolation and Gauss integration – Q8MEM [31]. The

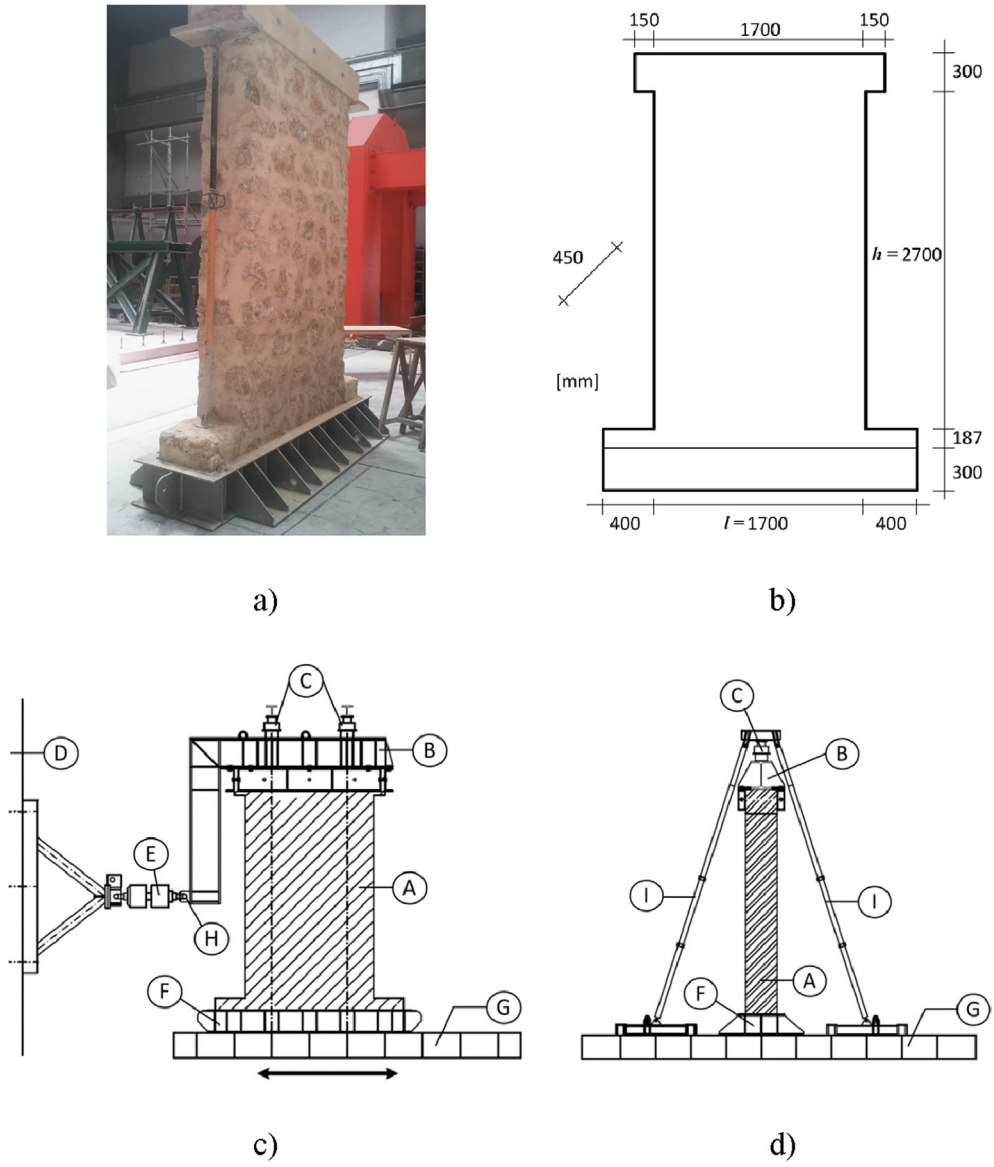

Fig. 1. Experimental specimens: a) construction of the specimens; b) geometry of the specimens [dimensions in mm]; c) test setup at LNEC – front view; d) test setup at LNEC – lateral view. (A) specimen; (B) "L" shaped top support; (C) vertical actuators; (D) reaction wall; (E) horizontal load cell; (F) bottom support; (G) shaking table; (H) fixed horizontal translation; (I) steel anchors for applying the vertical load.

springs were simulated using unidirectional single-point elements – SP1TR [31]. The stiffness of these springs (Table 3) was estimated taking into account the cross sectional area of the steel tubes used as anchors in the experimental setup. The final finite element mesh can be seen in Fig. 4b and it is composed of 3223 elements and 3403 nodes. The steel components were considered linear elastic, and reference values were used, being 210 GPa for the Young's Modulus (E) and 0.3 for the Poisson coefficient (υ). The mechanical properties for masonry will be addressed during the model calibration process.

In order to properly replicate the experimental campaign, it was necessary to use phased analyses [31], meaning that in a first phase the model experiences its self-weight and the vertical load, being during this phase, constraint in the horizontal direction. In a second phase, and maintaining the deformation and stress state, the springs on the top of the model are activated. During this second phase the base of the model experiences the horizontal displacement. During the experimental testing it was possible to observe some rotation of the model (coming from the steel anchors and the support steel structure itself). This was also possible to see in the numerical model due to the inclusion of the steel support and the springs acting as the steel anchors. Similar to the experimental specimens, the horizontal force is recorded as the horizontal reaction of the steel L-shaped structure on the top of the wall (corresponding to the "H" point of Fig. 1). The horizontal displacement is measured at the same heights as the LVDTs in the experimental tests.

3.1. Non-linear behaviour

Because masonry exhibits non-linear behaviour, a Total Strain Crack (TSC) model was selected. These models, which describe the tensile and compressive behaviour of the material with one stress–strain relation, are usually adequate for this purpose [31]. For ancient and irregular masonry isotropic models are usually adopted [13]. The TSC models can be categorized into fixed (TSFC) and rotating (TSRC) smeared crack models. In both formulations, the crack is initiated when the maximum principal stress equals

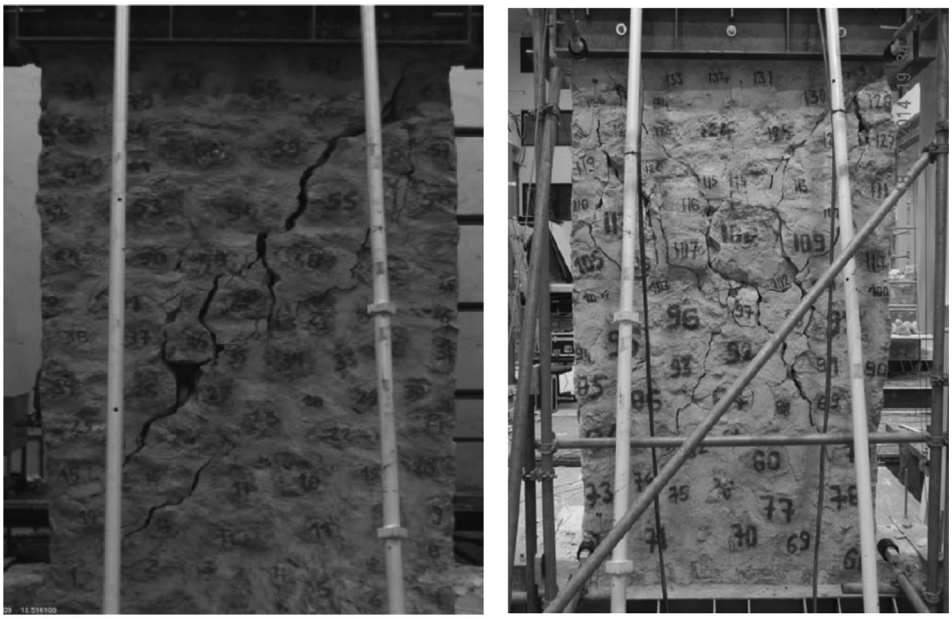

Fig. 2. Failure modes for the experimental walls: a) Wall 1; b) Wall 2.

the tensile strength of the material, and its initial orientation is normal to the maximum principal strain. The main difference between these two formulations is related to the crack orientation during the inelastic process. In the TSFC model, the coordinate system is fixed upon cracking according to the principal strain directions and remains invariant during the total analysis process. Each integration point admits a maximum of two orthogonal cracks. The TSRC model allows a gradual correction of the initial crack direction, as the crack plane can rotate during the analysis. The crack direction rotates with the principal strain axes, ensuring that the crack remains normal to the direction of the maximum principal strain. In the fixed formulation, a shear retention parameter is required for the definition of the model shear behaviour, while in the rotating model the shear softening occurs implicitly as a result of the principal stress and strain conditions. Although some studies [32–35] showed that for shear dominated applications, the rotating model resulted in more realistic predictions while the fixed model tended to behave too stiff, more recent studies have shown that TSFC model are also capable of predicting the behaviour in shear dominant applications [36–37]. For the purpose of this work, the TSRC model was used. Parabolic behaviour for compression (Fig. 5a) and exponential behaviour for tension (Fig. 5b) were used to describe the post-peak behaviour of the masonry [31].

In order to use these constitutive models, it is necessary to define a set of parameters related to the mechanical properties of the material. Initially, some reference values for the mechanical properties of ancient masonry were used [26]. Later, the obtained results are compared with the experimental results and the initial input values are updated in sequence. The calibration process starts with the elastic part (Young's modulus), then the compressive properties (compressive strength and compressive fracture energy) and lastly the tensile properties (tensile strength and tensile fracture energy). This is a calibration process in which the objective is to approximate the numerical results with the experimental results. The steel behaviour was kept elastic due to the considerable difference in stiffness when compared with the masonry. The equilibrium solution of the equations in each step of the nonlinear analysis is obtained using a regular Newton-Raphson iterative method and a convergence criterion based on internal energy with a tolerance of 10^{-3}.

3.2. Model calibration

Different experimental specimens were tested and presented previously. From the experimental results it was possible to see that the shear resistance of the experimental specimens is similar in monotonic and cyclic conditions. In order to simplify the numerical analysis, these models were only simulated under monotonic conditions, imposing a horizontal loading until failure.

The FEM model corresponds to Wall 1. This specimen was tested under monotonic loading and had an initial vertical load of 0.15 MPa. Table 1 shows the mechanical properties after the calibration process. The obtained values for the different mechanical properties can be considered in the expected range. As an example, the Italian Standard [38] suggests values for the compressive strength of this kind of masonry up to 0.9 MPa which is quite close to the presented 1.03 MPa.

The approximation of the numerical results with the experimental results can be seen in Fig. 6a where both force–displacement curves can be compared. The obtained numerical curve shows a good agreement with the experimental curve. The shear resistance of the numerical model is 105.9 kN (less than 1% difference comparing to the experimental result). This value was obtained at a displacement of 8.91 mm (less than 1% difference comparing to the experimental result). Besides the force–displacement curves, also the damage pattern and the failure mode were compared. In the case of the numerical model the maximum principal strains were used as an indicator for cracking. A comparison of the damage patterns of both experimental and numerical models can be seen in Fig. 6b. From the numerical analysis it is possible to see a shear failure with diagonal cracking, which is the same observation obtained for the experimental specimen.

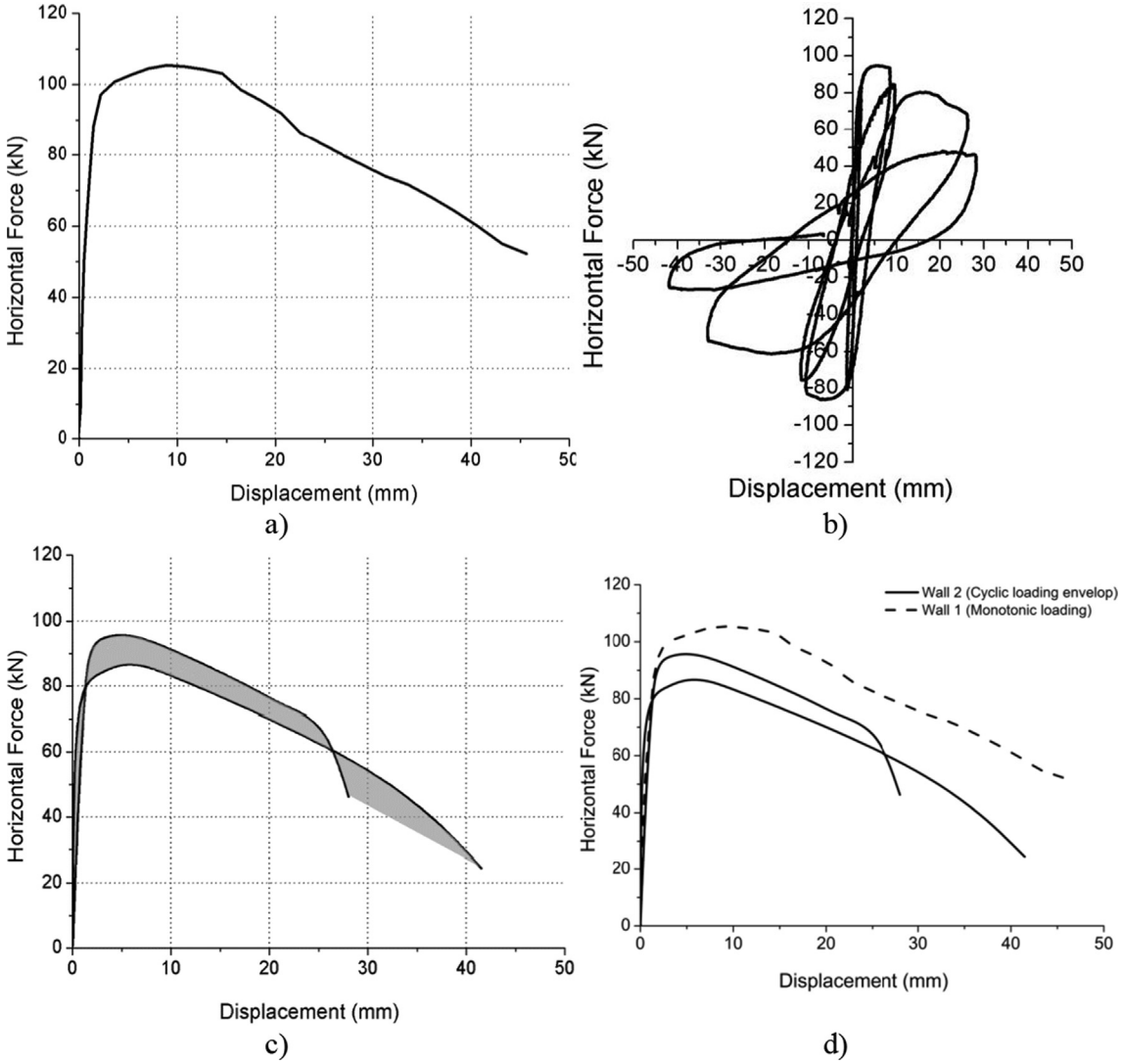

Fig. 3. Force-displacement curves for the experimental specimens: a) Wall 1 under monotonic loading; b) Wall 2 under cyclic loading; c) Envelop of the cyclic test for Wall 2; d) comparison between both walls.

3.3. Parametric studies

In order to clarify the influence and the interactions between different aspects of rubble stone masonry walls, a comprehensive parametric study was conducted using the calibrated numerical model already presented. The authors would like to point out that, although the modelling strategy adopted within this work has proven to be quite successful in predicting the behaviour of masonry walls [25–30], this calibrated numerical model was only calibrated based on the available experimental results (Section 2), thus the results obtained with different geometries, different material properties or different failure modes, should be analysed considering this limitation. The studied aspects were: a) geometry of the wall, focusing on the *h*/*l* relation; b) vertical load, as a function of the masonry's compressive strength; c) support conditions, adopting different stiffness supports at the top of the wall; and d) mechanical properties (Table 2). Regarding the geometry, four *h*/*l* relations were studied ranging from 0.6 to 2.0. Three different vertical loads were applied ranging from 5% to 25% of the compressive strength of masonry. Different stiffness supports were introduced adding different height spandrels on top of the wall, these varied from 250 mm to 750 mm. The mechanical properties obtained for Wall 1 were the basis (M1) for this parametric studies and were changed ± 25%. It should be noted that all mechanical properties were affected by this coefficient. All of these parameters were combined and 108 new numerical models were developed.

It should be noted that in these new models the springs and the steel support structure on the top of the wall were removed, as the support conditions were changed and were in fact one of the parameters under the scope of this study. Instead, new elements (spandrel with variable height) were added to the model on top of the wall and its free edge had its rotations blocked (Fig. 7). With these new conditions, these models are initially loaded with their self-weight and vertical load and later a horizontal loading is applied until failure. The same constitutive models and method for solving the non-linear equations are applied. The new numerical models were built with the same elements (Q8MEM) and the same mesh density.

The different *h*/*l* relations were obtained maintaining the same height of the wall and varying the length. Increasing the wall length, with the height unchanged, will change the slenderness, but it will also change the wall cross sectional area, in fact changing also the design area. In order to isolate this effect, the force was normalized (dividing the force by the horizontal cross sectional

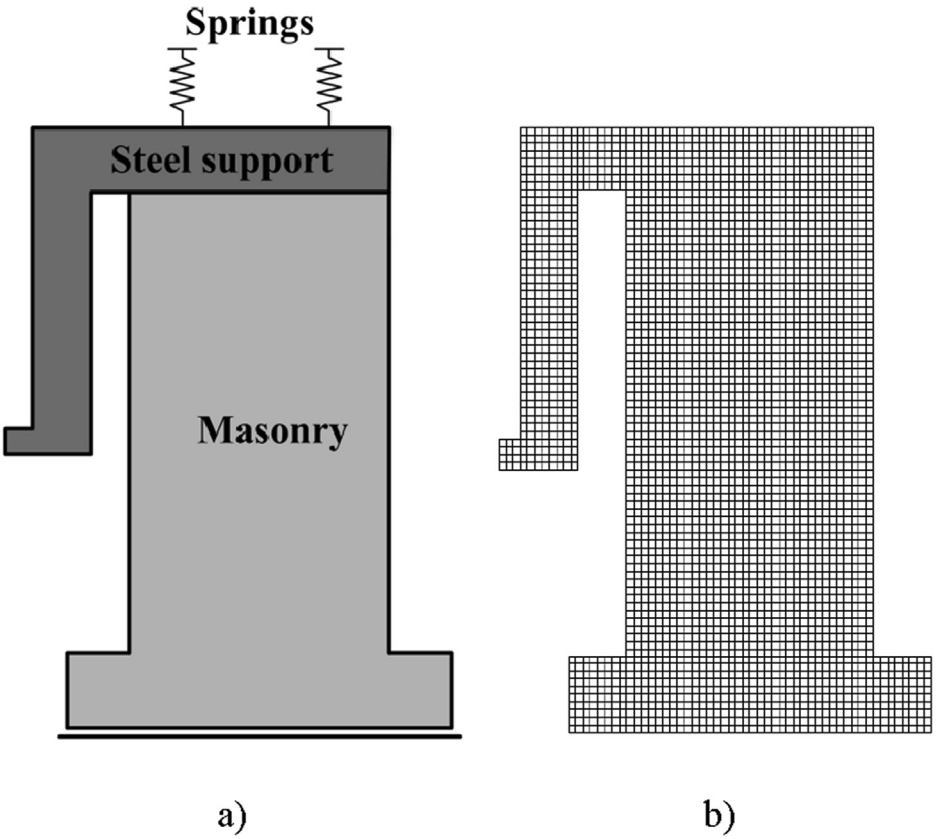

Fig. 4. Numerical models: a) schematic representation; b) finite element mesh.

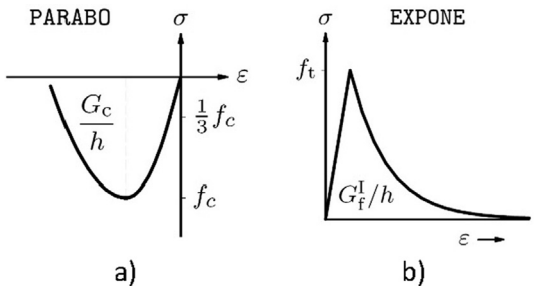

Fig. 5. Masonry constitutive model: a) Parabolic compressive softening; b) Exponential tensile softening [31].

Table 1
Calibrated mechanical properties for the numerical model.

Property	Wall 1
Young's Modulus, E (GPa)	1.750
Compressive strength, f_c (MPa)	1.030
Fracture energy in compression, G_c (N/mm)	9.000
Tensile strength, f_t (MPa)	0.060
Mode-I Fracture energy, G_f (N/mm)	0.250
Density, γ (kg/m3)	1900
Stiffness (springs), K (kN/m)	4.5E + 06

area). Fig. 8 shows the force–displacement curves for all considered geometries, for different pre-compression levels, keeping the mechanical properties as M1 and a 500 mm spandrel.

It is possible to see that the geometry of the wall has a considerable influence on the maximum shear capacity. When changing the *h/l* relation from 0.6 to 1.0 it is possible to see a decrease in the maximum shear capacity of 25%. This decrease is similar when changing the *h/l* from 1.0 to 1.6. This reduction in the maximum shear capacity is less pronounced for higher *h/l* relations, being only 16% when changing from 1.6 to 2.0 (*h/l*), as can be seen in Fig. 8d, where it is possible to compare the maximum shear capacities for different *h/l* relations for different vertical loadings. These were obtained keeping the mechanical properties as M1 (Table 2) and a 500 mm spandrel. Besides the force–displacement curves, also the failure modes were analysed. Keeping all other parameters unchanged, it was possible to see that for lower slenderness values the most common failure mechanism is through shear with diagonal cracking, whereas for higher slenderness values the failure mode tends to change for flexure mechanism with toe crushing and rocking (Fig. 9).

Three different vertical loadings were considered as a function of the compressive strength of the masonry and varied from 5% to 25%. It is known that the pre-compression level influences the initial stiffness of the wall [16,17,19,22,39,40] however, in order to isolate the effect of the pre-compression level, the initial stiffness of the walls was not changed when changing the vertical loading. This should be taken into account when analysing these results. Fig. 10 shows the force–displacement curves for all the considered pre-compression levels. As expected, the pre-compression level influences the response of these structural elements. When the vertical load decreases from 25% to 15% of the compressive strength, there is an average decrease of the maximum shear capacity of about 18%, whereas there is an average decrease of 33% of the maximum shear capacity when the vertical load decreases from 15% to 5% of the compressive strength. These were obtained keeping the mechanical properties as M1 (Table 2) and a 500 mm spandrel. The failure mechanism where also analysed, and in Fig. 11 some examples are presented. It is possible

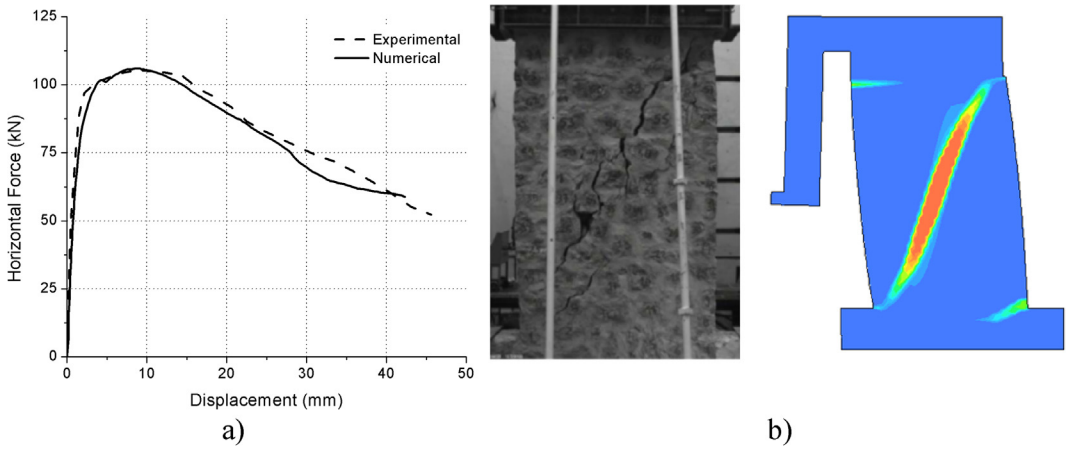

Fig. 6. Comparison between experimental and numerical results: a) force–displacement curve for Wall 1; b) damage pattern for Wall 1 (experimental and numerical).

Table 2
Range of the parametric study.

	Range			
Geometry (h/l)	0.6	1.0	1.6	2.0
Vertical loading (σ_v)	0.05f_c	0.15f_c		0.25f_c
Support conditions (spandrel height)	250 mm	500 mm		750 mm
Mechanical properties	0.75 M1	Model 1		1.25 M1

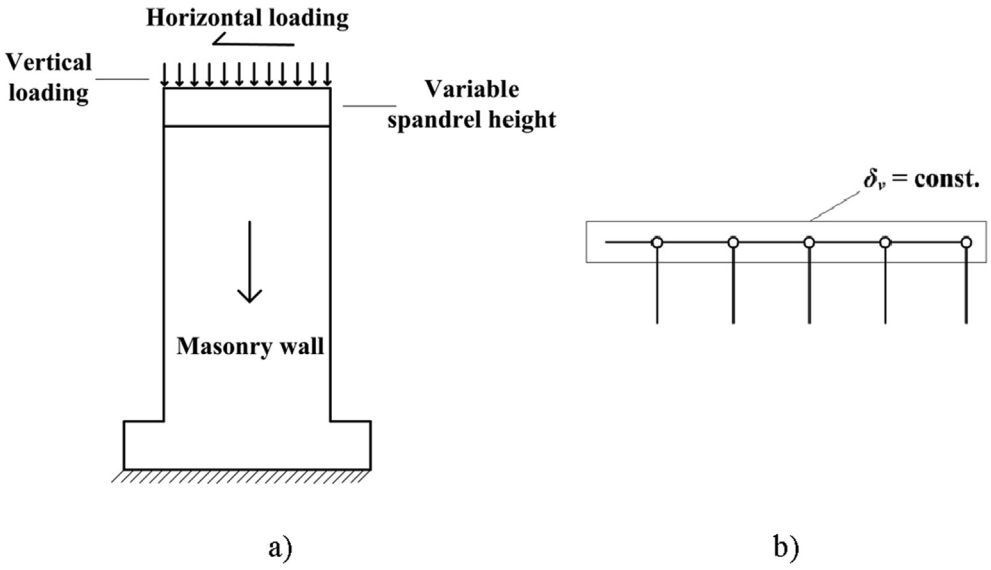

Fig. 7. Numerical models for the parametric study: a) general scheme; b) detail on the free edge of the spandrel.

to see that with the increase of the pre-compression level (vertical loading) the failure mechanisms tend to shift from flexural failure with toe crushing and rocking to shear failure with diagonal cracking.

The stiffness of the support was changed by varying the height of a spandrel on top of the wall. The free edge of the spandrel has its rotations blocked by making sure that all nodes of the free edge of the spandrel have the same vertical displacement (Fig. 7b). Three different heights of spandrel were considered, being 250 mm, 500 mm and 750 mm. It was possible to see that the height of the spandrel on top of the wall has little influence in the maximum shear capacity of the wall. For higher pre-compression levels this influence is even smaller. Changing from 250 mm to 750 mm height with a 5% pre-compression level increases the maximum shear capacity an average of 8%, while with a 25% pre-compression level only increases the shear capacity an average of 2% (considering all combinations of mechanical properties and h/l relations). The failure mechanism is also not influenced by the changes in the support stiffness. Although the stiffness of the supports has little influence in the maximum shear capacity and the failure mechanism of these walls, it should be pointed out that this aspect (support conditions) has shown to have a substantially influence in the drift capacity of these elements [24,40].

The mechanical properties from Wall 1 were used as a reference (M1) and two additional sets of ± 25% were created (Table 2). It was possible to see that the mechanical properties influence the maximum shear capacity of these elements. A 25% reduction in the

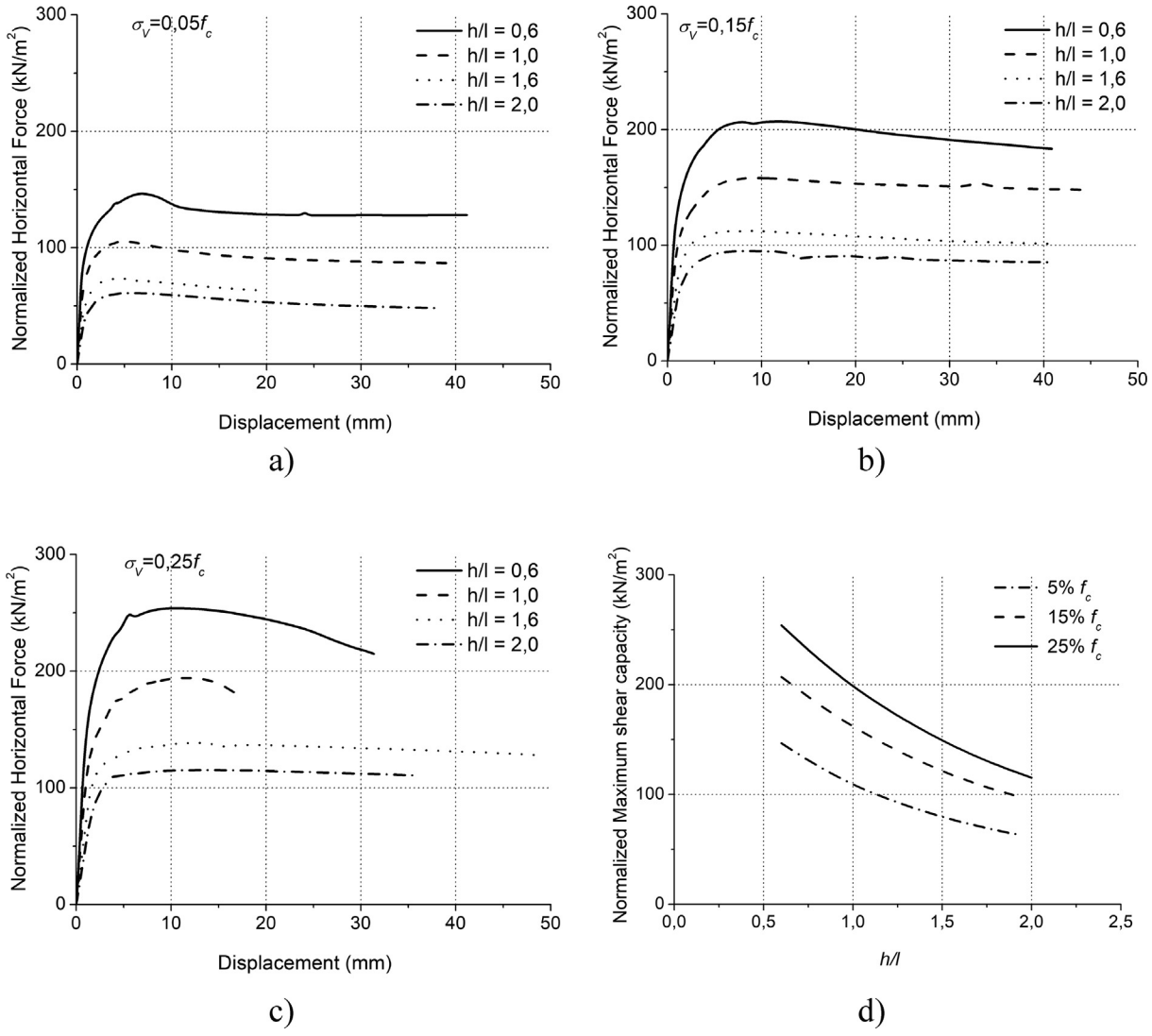

Fig. 8. Influence of geometry for different vertical loading (keeping the mechanical properties as M1 and a 500 mm spandrel): a) force–displacement curve for 5% compressive strength; b) force–displacement curve for 15% compressive strength; c) force–displacement curve for 25% compressive strength; d) normalized maximum shear capacity as a function of slenderness, for different vertical loadings.

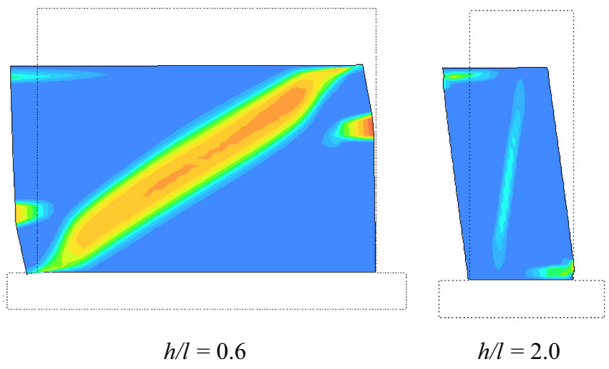

Fig. 9. Examples of failure mechanisms for different geometries.

mechanical properties showed a reduction in the maximum shear capacity between 9% and 23% with an average of 14%, while an increase of 25% in the mechanical properties showed an increase in the maximum shear capacity between 6% and 15% with an average of 10% (considering all combinations of *h*/*l* relations, spandrel height and pre-compression level). Besides the force–displacement curves, also the failure mechanism was analysed. It was possible to see that for lower mechanical properties the failure mechanisms tend to be governed by shear with diagonal cracking and for higher mechanical properties the failure mechanism tends to be governed by flexure with toe crushing and rocking. This was possible to observe for all the pre-compression levels and geometric configuration under the scope of this work.

4. Analytical study

Several studies have been conducted with the objective of predicting the in-plane shear resistance of these structural elements through analytical solutions derived from experimental studies [41]. In this section the in-plane shear capacity of the above numerical models will be estimated accordingly to the existing documentation: a) Eurocode 6 – EC6 [42]; b) Italian Standard – NTC18 [38]; c) American Standard – FEMA [43]; and d) New Zealand Standard – NZSEE [44]. All these analytical methods consider the shear behaviour of walls by equations to estimate the strength capacity of the walls according to the failure mode. The analytical

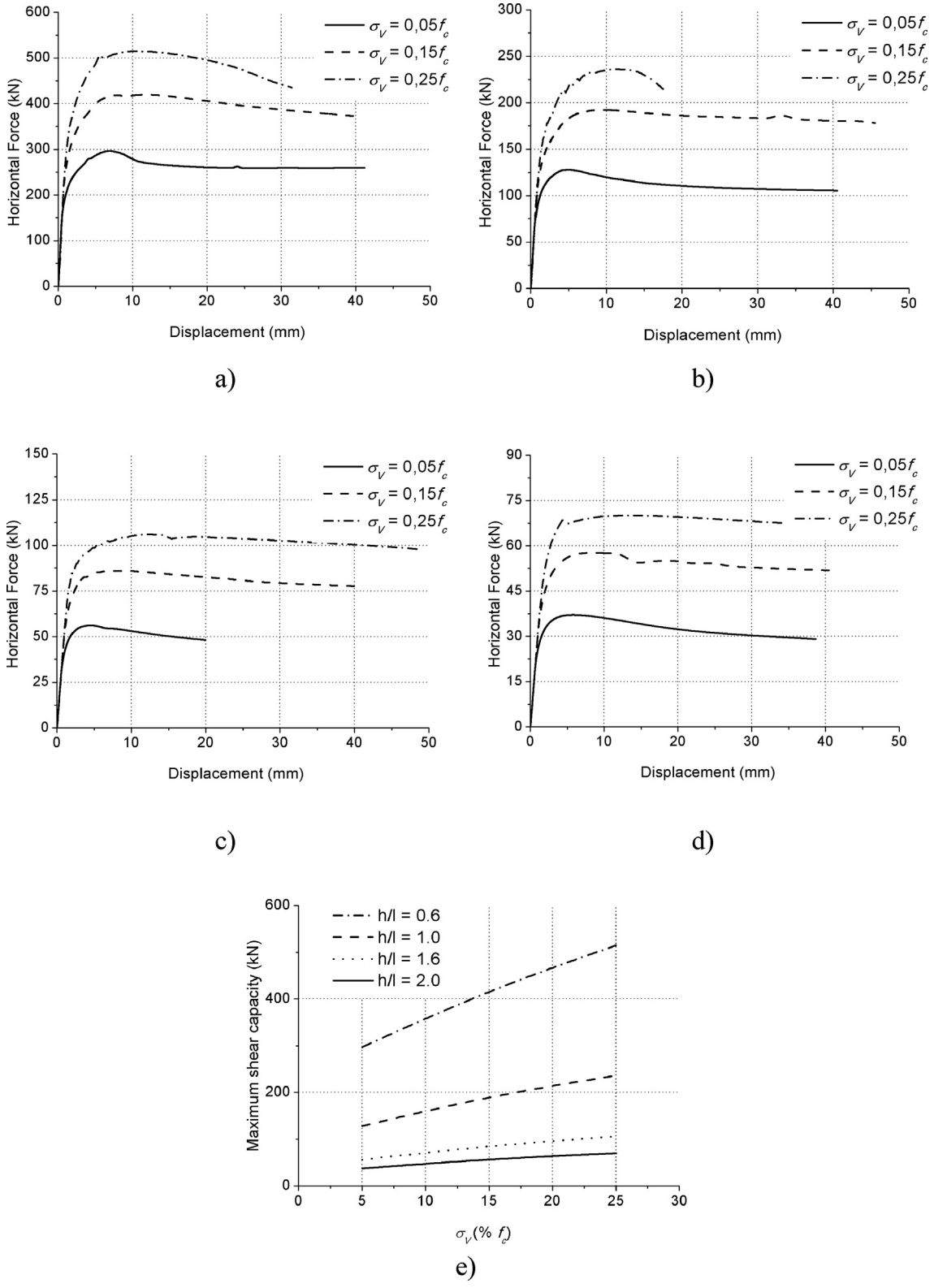

Fig. 10. Influence of pre-compression level for different geometries loading (keeping the mechanical properties as M1 and a 500 mm spandrel): a) force–displacement curve for h/l = 0.6; b) force–displacement curve for h/l = 1.0; c) force–displacement curve for h/l = 1.6; d) force–displacement curve for h/l = 2.0; e) maximum shear capacity as a function of pre-compression level, for different geometries.

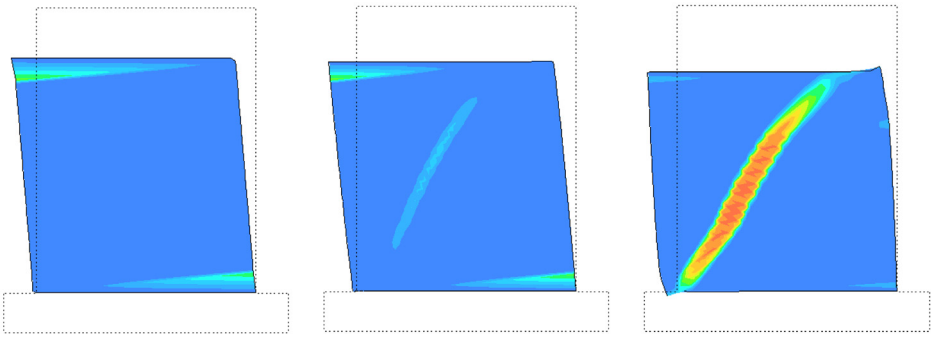

Fig. 11. Examples of failure mechanisms for different pre-compression levels.

equations are discussed and the in-plane capacity is compared with the numerical results. The final analytical solutions from all the considered standards can be seen in Table 3.

4.1. EC6 equations

The in-plane resistance of walls, according to EC6 [42], is the minimum strength of the considered failure modes. It should be pointed that this standard doesn't prescribe for rubble masonry walls. Nonetheless this standard was also studied and applied in order to see if the prescribed analytical solutions can be applied also to rubble masonry walls.

The lateral resistance of a wall where the failure is controlled through toe crushing is defined by the crushing of the compressed area in the bottom corner, not considering the tensile strength of masonry [11]. The stress distribution is commonly assumed as an equivalent rectangular stress block with a coefficient equal to 0.85 [11]. With this stress equilibrium is possible to develop an equation able to estimate the lateral resistance of these elements with this failure mechanism [11] – Eq. 1.

The European standard [42] only considers, in the case where shear mechanism are the dominant ones, the sliding of the bed-joint. This mechanism occurs when the acting shear stress in the effective section exceeds the shear resistance of the bed-joint. The shear resistance can be determined according to Mohr-Coulomb formulation assuming the effective uncracked section length [10]. The length of the effective compression zone is calculated neglecting the masonry tensile strength and assuming a simplified distribution of compression stresses [10,11]. The equation is easily deducted by these relations – Eq. 2. This standard presents reference values for the cohesion of masonry; however, it doesn't provide values for rubble masonry. The lower value presented by [42] was selected for these analysis, being a cohesion of 0.1 MPa.

4.2. NTC18 equations

As the European standard, also this Italian standard [38] presents two analytical solutions to estimate the lateral resistance of wall, according to the failure mechanism. This standard provides prescriptions for rubble masonry and, it is in fact the only standard (of the selected) to contemplate this type of masonry.

According to this standard, the lateral resistance of walls where the failure is controlled through flexural mechanism follows the same principals of EC6 [42] – Eq. 1. In the case where the failure is controlled through shear mechanism this standard is different from the EC6 [42]. The latter presented a solution to determine the lateral resistance for the sliding of the bed-joint, while the Italian standard [38] considers the diagonal tension as the only shear failure mechanism, for existing masonry. This formulation assumes that the diagonal cracks are caused by the principal tensile stresses developing in the wall, with a critical value according to the tensile strength of masonry, and accounts for the influence of the geometric and load configuration. Assuming the masonry as an elastic, homogeneous and isotropic element, the lateral resistance of a wall failing in shear through diagonal cracking can be evaluated through Eq. 3. This standard presents reference values for the average shear strength of masonry (τ_0), being the value of 0.032 MPa selected for these analyses [38].

4.3. FEMA equations

FEMA [43] presents four analytical solutions to determine the lateral resistance of walls, according to the four possible failure

Table 3
Analytical expressions according to the failure mechanism.

	Flexural Strength		Shear Strength	
EC6 [42]	$V_F = \frac{M}{h_0} = \frac{N}{2h_0}\left(l - \frac{N}{0.85 f_c \cdot t}\right)$[Eq. 1]		$V_S = \frac{1.5 l \cdot t \cdot f_{v0} + 0.4N}{1 + \frac{3h_0 \cdot t \cdot f_{v0}}{N}}$[Eq. 2]	
NTC18 [38]	$V_F = \frac{M}{h_0} = \frac{N}{2h_0}\left(l - \frac{N}{0.85 f_c \cdot t}\right)$[Eq. 1]		$V_D = l \cdot t \frac{1.5\tau_0}{b}\sqrt{1 + \frac{N}{1.5\tau_0 \cdot l \cdot t}}$[Eq. 3] $b = 1.0 \le h/l \le 1.5$	
FEMA [43]	$V_R = 0.9\alpha \cdot N \frac{l}{h}$[Eq. 4]	$V_C = \alpha \cdot N \frac{l}{h}\left(1 - \frac{N}{0.7 f_c \cdot l \cdot t}\right)$ [Eq. 5] $\frac{l}{h} \ge 0.67$	$V_S = \frac{0.75\left(0.75 f_{v0} + \frac{N}{l \cdot t}\right)}{1.5} \cdot l \cdot t$[Eq. 6]	$V_D = f_t \cdot l \cdot t \frac{l}{h}\sqrt{1 + \frac{N}{f_t \cdot l \cdot t}}$[Eq. 7]
NZSEE [44]	$V_F = \frac{M}{h_0} = \frac{N}{2h_0}\left(l - \frac{N}{0.85 f_c \cdot t}\right)$[Eq. 1]		$V_S = \frac{1.5 l \cdot t \cdot f_{v0} + 0.4N}{1 + \frac{3h_0 \cdot t \cdot f_{v0}}{N}}$[Eq. 2]	$V_D^j = \frac{f_{v0} \cdot l \cdot t + \mu N}{1 + h_0/l}$[Eq. 8] $V_D^u = \frac{\sqrt{f_{ut} \cdot l \cdot t\left(f_{ut} \cdot l \cdot t + N\right)}}{2.3\left(1 + \frac{h_0}{l}\right)}$[Eq. 9]
	V_F – Flexural Strength V_R – Rocking Strength V_C – Toe Crushing Strength V_S – Sliding Strength V_D – Diagonal Tension Strength	V_D^j – Diagonal Tension Strength, joints V_D^u – Diagonal Tension Strength, units N – axial compressive force h_0 – effective height l – length	t – thickness f_c – compressive strength (masonry) f_t – tensile strength (masonry) b – coefficient for geometry α – coefficient for support conditions	f_{v0} – cohesion τ_0 – average shear strength of masonry μ – friction coefficient f_{ut} – tensile strength (units)

mechanisms. The lateral resistance of the wall is the minimum of the capacity calculated for each failure mechanism.

For rocking mechanism, a rotation over the lower corner of the wall is assumed. This standard introduces a factor of 0.9 for the calculation of the lateral resistance over this failure mechanism – Eq. 4. For toe crushing (Eq. 5) and diagonal tension (Eq. 7) the analytical solutions presented by this standard are similar to the European equations, however some differences can be found. For toe crushing the vertical stresses distribution in the compressed area is considered $0.7f_c$ instead of the $0.85f_c$ in the European documents. In the case of sliding mechanism, this standard also follows the Mohr-Coulomb criteria; however, it doesn't take into account the moment which implies that the reduction in the effective length due to the horizontal cracking is not considered – Eq. 6. This standard presents some reference values for the cohesion of masonry, however, like the EC6 [42], it doesn't contemplate rubble masonry. From the suggested values, a cohesion of 0.09 MPa was selected [43].

4.4. NZSEE equations

The NZSEE standard [44] presents one solution for walls failing under flexural mechanism with toe crushing and two solutions for walls failing under shear mechanism (sliding and diagonal tension).

The analytical equation for toe crushing mechanism (Eq. 1) and sliding (Eq. 2) follow the same principal as EC6 [42], already presented. The main difference of this standard consists in the differentiation of two possibilities when considering the mechanism of diagonal tension. Here, one solution is presented to account for the possibility of failure in the joints of masonry, following the Mohr-Coulomb principles (Eq. 8), and another solution is presented to account for the possibility of failure in the masonry units (Eq. 9). This document suggests some reference values for the cohesion, friction coefficient and the tensile strength of units. Because rubble masonry is not considered in this document, from the available values the following were selected: 0.1 MPa, 0.4 and 0.5 MPa for the cohesion, friction coefficient and tensile strength of units, respectively.

4.5. Analytical results

All these normative documents were applied to the numerical models (a total of 108) already presented and some examples can be seen in Table 4. The quality of the predictions was measured as the relation between the minimum predicted value from the analytical solutions and the obtained numerical value as $V_{min,predicted} / V_{num}$. Besides the lateral resistance of the wall, also the prediction of the failure mechanism was analysed.

The European standard [42] predictions ranged from 60% to 108%, with an average of 81%, relating to the numerical results. It should be noted that in only 3 cases (2.8%) the predictions from EC6 [42] gave higher strengths than the numerical values. This document was also able to correctly predict the failure mechanism in 70% of the models. In Fig. 12a it is possible to see that there is a slight improvement in the results (in terms of coefficient of varia-

Table 4
Examples (9 out of 108) of analytical models applied to the numerical models.

Model(h/l)(pre-comp. level)	Numerical [kN]	Formulation	Prediction [kN]					$\frac{V_{min,predicted}}{V_{num}}$	Same failure mode?
			Flexure		Shear				
			Rocking	Toe Crushing	Sliding	Diagonal Cracking			
#8(h/l = 2)(5% f_c)	53.60	EC6	42.52		42.94			0.79	yes
		NTC18	42.52		42.86			0.79	yes
		FEMA	43.27	44.30	64.09	46.69		0.81	yes
		NZSEE	42.52		42.94	59.28	100.57	0.79	yes
#16(h/l = 2)(15% f_c)	170.38	EC6	169.60		160.49			0.94	yes
		NTC18	169.60		132.91			0.78	yes
		FEMA	220.12	153.53	163.30	127.91		0.75	yes
		NZSEE	169.60		160.49	178.62	222.92	0.66	no
#30(h/l = 1)(5% f_c)	271.88	EC6	265.29		219.44			0.81	no
		NTC18	265.29		157.32			0.58	no
		FEMA	329.47	243.69	224.05	204.11		0.75	no
		NZSEE	265.29		219.44	178.62	222.92	0.66	no
#42(h/l = 1.6)(15% f_c)	141.53	EC6	111.69		93.31			0.66	no
		NTC18	111.69		102.86			0.73	no
		FEMA	110.77	109.25	102.55	139.71		0.72	no
		NZSEE	111.69		93.31	113.83	193.10	0.66	no
#64(h/l = 1)(15% f_c)	188.13	EC6	198.10		219.44			1.05	no
		NTC18	198.10		157.32			0.84	yes
		FEMA	329.47	162.10	224.05	151.67		0.81	yes
		NZSEE	198.10		219.44	178.62	222.92	0.95	yes
#71(h/l = 2)(15% f_c)	70.08	EC6	60.02		82.35			0.86	no
		NTC18	60.02		52.44			0.75	yes
		FEMA	82.37	71.39	112.02	44.72		0.64	yes
		NZSEE	60.02		82.35	66.98	83.59	0.86	no
#73(h/l = 1)(25% f_c)	265.46	EC6	289.14		204.30			0.77	yes
		NTC18	289.14		171.43			0.65	yes
		FEMA	307.70	277.84	170.91	273.84		0.64	yes
		NZSEE	289.14		204.30	218.89	371.35	0.77	yes
#94(h/l = 0.6)(15% f_c)	51.75	EC6	42.40		56.23			0.82	yes
		NTC18	42.40		44.30			0.82	yes
		FEMA	55.03	51.43	81.65	31.98		0.62	no
		NZSEE	42.40		56.23	54.83	78.20	0.82	yes
#104(h/l = 0.6)(15% f_c)	106.39	EC6	93.79		114.34			0.88	no
		NTC18	93.79		65.55			0.62	yes
		FEMA	128.70	89.23	140.03	69.88		0.66	yes
		NZSEE	93.79		114.34	93.03	116.10	0.87	yes

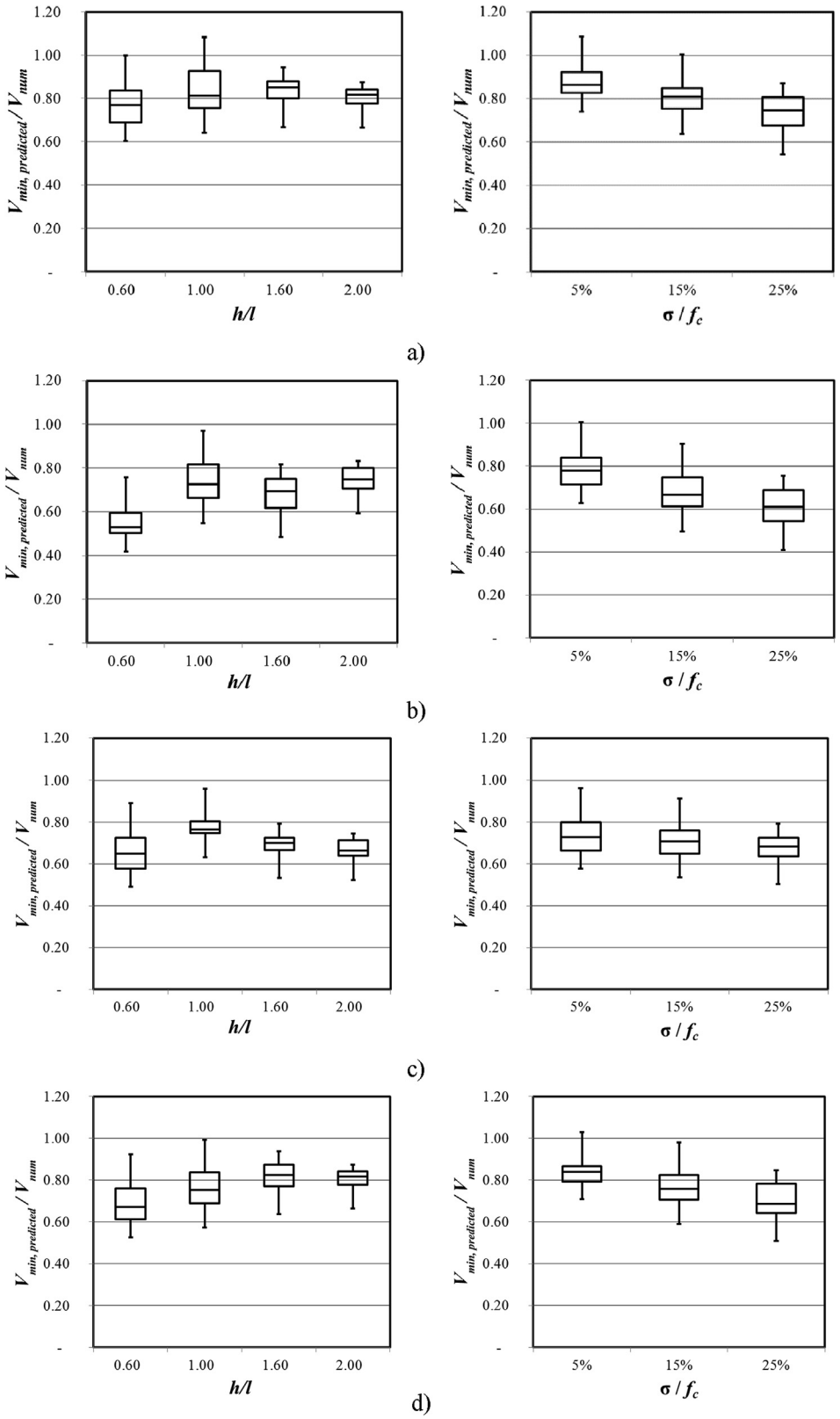

Fig. 12. Analytical predictions for different geometries and different pre-compression levels (showing minimum, quartile 1, quartile 2, quartile 3 and maximum values): a) using EC6 [42]: b) using NTC18 [38]; c) using FEMA [43]; d) using NZSEE [44].

tion) for walls with higher slenderness ratios. Fig. 12a also shows the quality of the results according to the pre-compression level. It is possible to see that the scatter is similar in all the range of vertical loads under study; however, it is possible to see that for lower pre-compression levels the results seem to be closer to the numerical ones. In fact, for a 5%f_c vertical load an average of 88% prediction was achieved, while for a 25%f_c vertical load only an average 74% prediction was achieved.

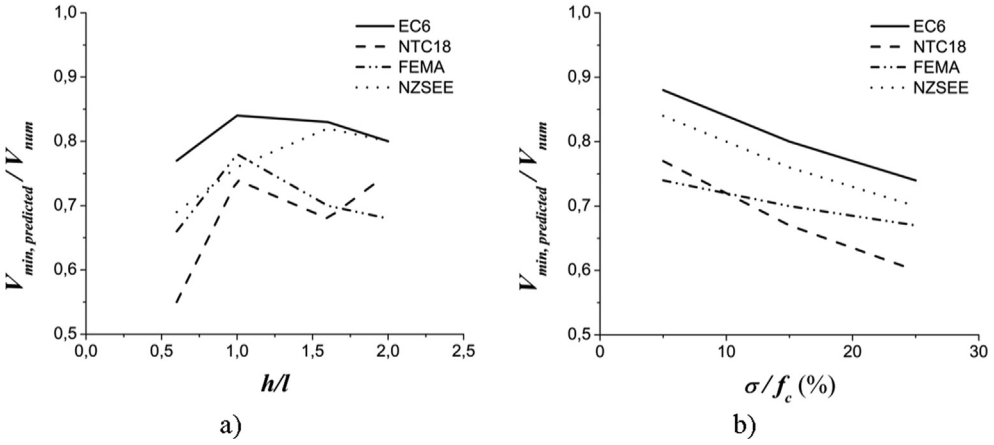

Fig. 13. Comparison of the average predictions: a) different geometries; b) different pre-compression levels.

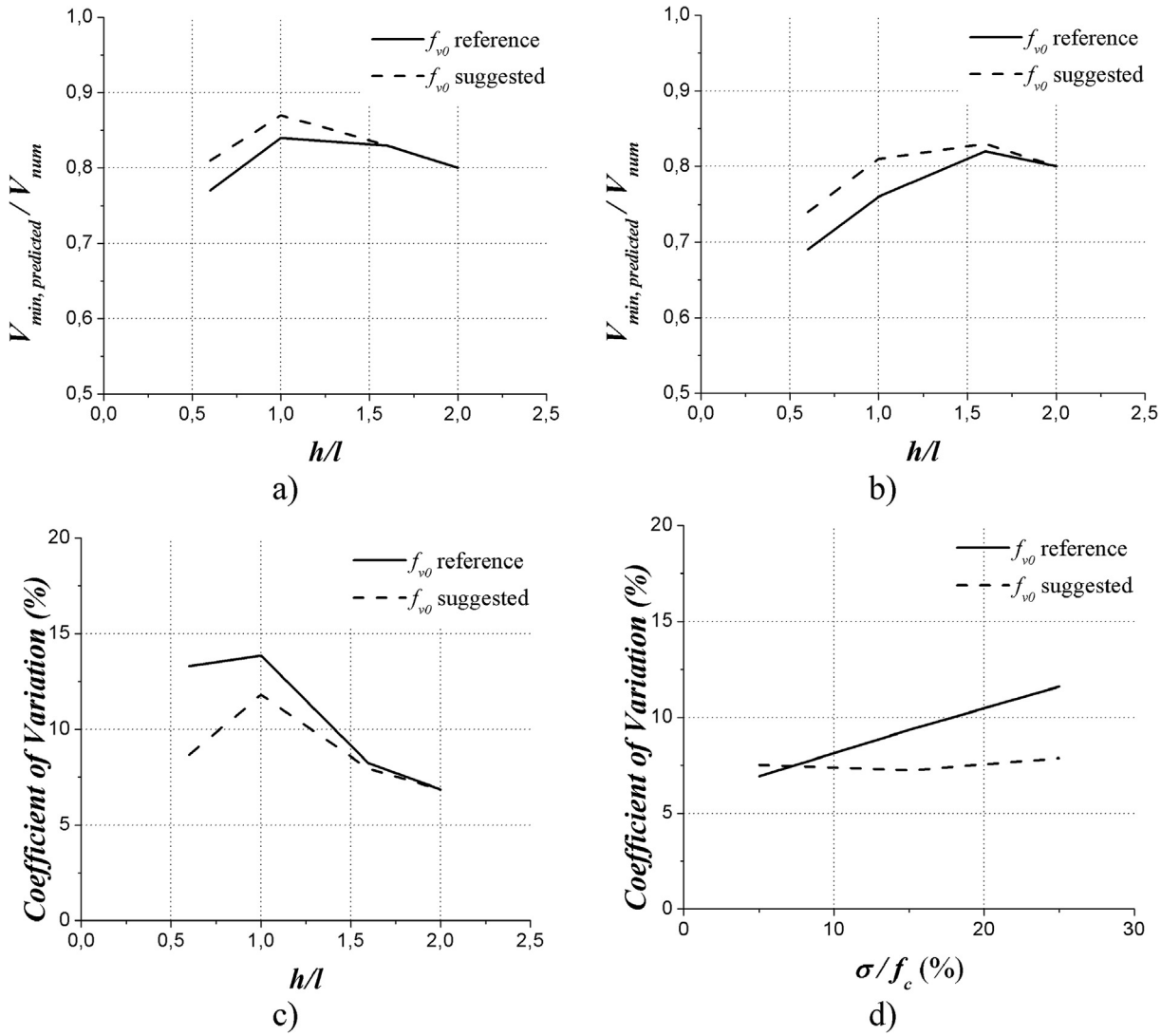

Fig. 14. The influence of the suggested masonry cohesion: a) influence in the prediction of the resistance for EC6 [42]; b) influence in the prediction of the resistance for NZSEE [44]; c) influence in the coefficient of variation for the predictions with EC6 [42]; d) influence in the coefficient of variation for the predictions with NZSEE [44].

The Italian standard [38] predictions ranged from 44% to 95%, with an average of 68%. This document was also able to correctly predict the failure mechanism in 55% of the models. The weakest results obtained with this standard were for the lower slenderness ratio wall (h/l = 0.6) with an average of 55% (Fig. 12b). The American standard [43] predictions ranged from 50% to 91%, with an

average of 71%. This document was also able to correctly predict the failure mechanism in 50% of the models (Fig. 12c). The New Zealand standard [44] predictions ranged from 56% to 98%, with an average of 77%. This document was also able to correctly predict the failure mechanism in 66% of the models (Fig. 12d). The behaviour of these predictions according to the geometry of the wall and the pre-compression level is similar to the previous standards, lower coefficients of variation for slender walls and higher average predictions for lower pre-compression levels.

Fig. 13 shows a comparison of the average of predictions for all studied standards. It is possible to see that globally the EC6 [42] and the NZSEE [44] present the analytical solutions that better predicted the numerical results. These two standards were also the ones that had the higher number of correctly predicted failure mechanisms.

Because most of the available standards don't prescribe specifically for stone rubble masonry, selecting reference values for mechanical properties is not straightforward. One of the mechanical properties that had to be chosen from reference values was the masonry cohesion, being required for most of the available analytical solutions. Being so, the authors suggest that the cohesion could be related to the masonry tensile strength in the following equation:

$$f_{v0} = 2f_t \tag{10}$$

Using equation (Eq. (10)) instead of the available values (from the standards) and recalculating the analytical solutions presented earlier it is possible to see an improvement in the results. There is an overall increase in the predictions averages for all the studied standards, as can be seen in Fig. 14a,b, where a comparison between the averages of the predictions is presented for the EC6 (Fig. 14a) and NZSEE (Fig. 14b). It should be noted that there is an improvement, not only on the average of the predictions, but also in the quality of the results, meaning that lower coefficients of variation were obtained (Fig. 14c,d).

5. Discussion and conclusions

The behaviour of stone rubble masonry walls when subjected to horizontal loads was studied in this paper. This study involved experimental, numerical and analytical analysis of different walls under different conditions.

The experimental campaign was developed at LNEC (National Laboratory for Civil Engineering, Portugal) and involved full scale rubble stone masonry walls built and tested under different conditions. These tests served as a calibration base for the numerical study. The comparison between the numerical and the experimental capacity curves and damage distribution allowed concluding that the numerical models were able to reproduce the experimental in-plane behaviour of these walls. The maximum horizontal load was well estimated (with a 1% difference) and the plastic strains evolution accurately described the experimental failure modes.

The calibrated numerical models seem capable of predicting the behaviour of these elements when subjected to both vertical and lateral load. The calibrated mechanical properties for Wall 1 are within the expected range for this kind of structural element.

In order to study the influence of different parameters in the response of these structural elements, an extensive parametric study was performed and presented. It was shown that the geometry and the pre-compression level acting on the wall are the parameters with the most influence in the shear behaviour of these elements, both in terms of the maximum shear capacity and the failure mechanism. It was also possible to see that for this kind of walls the stiffness of the support doesn't influence the maximum shear capacity of these walls, however, it should be noted that this parameter has been reported [24,40] as having some influence in the post-peak behaviour affecting the obtained drift. In this case, because of the obtained mechanical properties, it was not possible to verify this phenomenon. Varying the mechanical properties of these models also affects the shear behaviour. A 25% variation in the mechanical properties (all properties) leads to a variation between 6% and 23% (considering all combinations of vertical load and geometry of the wall) of the maximum shear capacity of these structural elements.

Four different analytical solutions were studied, presented, applied and compared with the numerical and experimental results obtained before. It was possible to see that the analytical models, in general, achieved better predictions for lower pre-compression levels, and also for slender wall. It was observed that for these rubble stone masonry walls the EC6 [42] and the NZSEE [44] were the standards with the better predictions in terms of both the maximum shear capacity and the failure mechanism. It should be noted that these are related. The fact that these two standards were able to predict the correct failure mode in more cases (70% and 66% for EC6 [42] and NZSEE [44], respectively) led to a better overall prediction of the maximum shear capacity. Because most of the available standards don't take into consideration rubble stone masonry, a new equation for estimating the masonry cohesion was suggested. With the new cohesion introduced in the analytical models, the obtained results improved, not only in the average prediction, but also in lowering the coefficients of variation of the obtained results.

CRediT authorship contribution statement

João M. Pereira: Formal analysis, Writing - original draft. **António A. Correia:** Resources, Writing - review & editing. **Paulo B. Lourenço:** Supervision, Writing - review & editing.

Declaration of Competing Interest

The authors declare that they have no known competing financial interests or personal relationships that could have appeared to influence the work reported in this paper.

Acknowledgement

This work was performed under the research project: EpiCidade – Development of strengthening methods and experimental dynamic analysis of masonry buildings, with the reference QREN 13/SI/2011.

References

[1] D.P. Abrams, Performance-based engineering concepts for unreinforced masonry building structures, Prog. Struct. Engng Mater. 3 (1) (2001) 48–56.
[2] S. Lagomarsino, On the vulnerability assessment of monumental buildings, Bull Earthquake Eng 4 (4) (2006) 445–463.
[3] A. Furukawa, J. Kiyono, Casualty estimation in the collapse of masonry structures due to earthquakes, Prot. Hist. Build. Prohitech. 09 (2009) 423–429.
[4] M. Betti, A. Vignoli, Assessment of seismic resistance of a basilica-type church under earthquake loading: Modelling and analysis, Adv. Eng. Softw. 39 (4) (2008) 258–283.
[5] M. Corradi, A. Borri, A. Vignoli, Strengthening techniques tested on masonry structures struck by the Umbria–Marche earthquake of 1997–1998, Constr. Build. Mater. 16 (4) (2002) 229–239.
[6] A. Dagangun, H. Sezen, R. Livaoglu, A. Do, Performance evaluation of historical masonry manumental structures during the 1999 Turkey earthquakes, Prot. Hist. Build. Prohitech. 09 (2009) 1465–1470.
[7] T. Sturm, M. Astroza, G.R. Saragoni, Vulnerability analysis of two centennial buildings that survived undamaged the two large Valparaiso earthquakes of 1906 and 1985, Prot. Hist. Build. Prohitech. 09 (2009) 1547–1552.
[8] Moon, FL. (2004) Seismic strengthening of low-rise unreinforced masonry structures with flexible diaphragms. Georgia Institute of Technology.

[9] C. Calderini, S. Cattari, S. Lagomarsino, In-plane strength of unreinforced masonry piers, Earthquake Eng. Struct. Dyn. 38 (2008) 243–267.
[10] G. Magenes, G.M. Calvi, In-plane seismic response of brick masonry walls, Earthquake Engng. Struct. Dyn. 26 (11) (1997) 1091–1112.
[11] M. Tomazevic, Earthquake-resistant design of masonry buildings, Imperial College Press, 1999.
[12] V. Mallardo, R. Malvezzi, E. Milani, G. Milani, Seismic vulnerability of historical masonry buildings: A case study in Ferrara, Eng. Struct. 30 (8) (2008) 2223–2241.
[13] P.B. Lourenço, Computations on historic masonry structures: HISTORIC MASONRY STRUCTURES, Prog. Struct. Engng Mater. 4 (3) (2002) 301–319.
[14] Anthoine, A., Magonette, G., Magenes, G. (1995) Shear-compression testing and analysis of brick masonry walls. In 10th European Conference on Earthquake Engineering, pp. 1657-1662.
[15] Oliveira, DV. (2003) Experimental and numerical analysis of blocky masonry structures under cyclic loading. University of Minho.
[16] G. Vasconcelos, Experimental investigation on the mechanics of stone masonry: characterization of granites and behaviour of ancient masonry shear walls, University of Minho, 2005.
[17] Seki, M., Vacareanu, R., Saito, T., Cotofana, D. (2008) Cyclic shear tests on plain and FRP retrofitted masonry walls. In: 14th World Conference on Earthquake Engineering.
[18] Magenes, G., Morandi, P., Penna, A. (2008) Experimental in-plane cyclic response of masonry walls with clay units. In: 14th World Conference on Earthquake Engineering.
[19] A. Elmenshawi, M. Sorour, A.A. Mufti, In-plane seismic behavior of historic stone masonry, Can. J. Civ. Eng. 37 (2010) 465–476.
[20] Magenes, G., Penna, A., Galasco, A., Da Pare, M. (2010) In-plane cyclic shear tests of undressed double-leaf stone masonry panels. In: 8th International Masonry Conference.
[21] R. Capozucca, Shear Behaviour of Historic Masonry Made of Clay Bricks, TOBCTJ 5 (1) (2011) 89–96.
[22] B.L. Silva, Diagnosis and strengthening of historical masonry structures: numerical and experimental analysis, University of Brescia, 2012.
[23] Churilov, S., Dumova-Jovanoska, E. (2013) In-plane shear behaviour of unreinforced and jacketed brick masonry walls. Soil Dynamics and Earthquake Engineering 50, pp. 85-105.
[24] A. Araujo, Modelling of the seismic performance of connections and walls in ancient masonry buildings, University of Minho, 2015.
[25] P.B. Lourenço, Computational strategies for masonry structures, Delft University of Technology, 1996.
[26] Lourenço, PB. (2009a) Recent advances in masonry modelling: micromodelling and homogenization. In: Multiscale Modelling in Solid Mechanics, pp. 251-294.
[27] L. Berto, A. Saetta, R. Scotta, R. Vitaliani, Shear behaviour of masonry panel: parametric FE analysis, Int. J. Solids Struct. 41 (2004) 4383–4405.
[28] M. Betti, A. Vignoli, Modelling and analysis of a Romanesque church under earthquake loading: Assessment of seismic resistance, Eng. Struct. 30 (2) (2008) 352–367.
[29] D. Abruzzese, L. Miccoli, A. Vari, Dynamic investigations on medieval masonry towers: vibration measurements and structural identification, Prot. Hist. Build. Prohitech 09 (2009) 807–813.
[30] M. Annecchiarico, F. Portioli, R. Landolfo, FE simulation of masonry wall samples of Mustafa Pasha mosque by homogeneous continuum models: analysis and calibration, Protect. Hist. Build. Prohitech. 09 (2009) 95–100.
[31] TNO DIANA (2009) DIANA, Displacement methods ANAlyser, release 9.4, User's Manual.
[32] P.B. Lourenço, J.G. Rots, Multisurface Interface Model for Analysis of Masonry Structures, J. Eng. Mech. 123 (7) (1997) 660–668.
[33] J.G. Rots, Computational modelling of Concrete Fracture, Delft University of Technology, 1988.
[34] Balakrishnan S., Murray D.W., "Prediction of response of concrete beams and panels by nonlinear finite element analysis", IABSE Reports 54, Coll. Comp. Mech. of Reinforced Concrete, Delft Univ. Press, 393-404 (1987)
[35] Kollegger J., Mehlhom G., "Material model for cracked reinforced concrete", IABSE Reports 54, Coll. Comp. Mech. of Reinforced Concrete, Delft Univ. Press, 63-74 (1987)
[36] M. Soltani, X. An, K. Maekawa, Localized nonlinearity and size-dependent mechanics of in-plane RC element in shear, Eng. Struct. 27 (6) (2005) 891–908.
[37] E. Michelini, P. Bernardi, R. Cerioni, B. Belletti, Experimental and Numerical Assessment of Flexural and Shear Behavior of Precast Prestressed Deep Hollow-Core Slabs, Int. J. Concr. Struct. Mater. 14 (1) (2020), https://doi.org/10.1186/s40069-020-00407-y.
[38] NTC18 (2018) Technical regulations for the construction. Italian ministry of the infrastructure.
[39] G. Magenes, G.M. Calvi, Cyclic behaviour of brick masonry walls, in: In: 10th World Conference in Earthquake Engineering, 1992, pp. 3517–3522.
[40] S. Petry, K. Beyer, Influence of boundary conditions and size effect on the drift capacity of URM walls, Eng. Struct. 65 (2014) 76–88.
[41] T. Yi, Experimental investigation and numerical simulation of an unreinforced masonry structure with flexible diaphragms, Georgia Institute of Technology, 2004.
[42] EC6-3 (2005) Eurocode 6 – design of masonry structures – Part 3: simplified calculation methods for unreinforced masonry structures.
[43] FEMA 356 (2000) Prestandard and commentary for the seismic rehabilitation of buildings. Federal Emergency Management Agency.
[44] NZSEE (2006) Assessment and improvement of the structural performance of buildings in earthquakes.